Biosensors and Bioelectronics 64 (2015) 404–410

Contents lists available at ScienceDirect

Biosensors and Bioelectronics

journal homepage: www.elsevier.com/locate/bios

Dopamine fluorescent sensors based on polypyrrole/graphene quantum dots core/shell hybrids

Xi Zhou [a], Peipei Ma [a], Anqi Wang [a], Chenfei Yu [a], Tao Qian [a], Shishan Wu [a,*], Jian Shen [a,b,**]

[a] School of Chemistry and Chemical Engineering, Nanjing University, Nanjing 210093, China
[b] Jiangsu Collaborative Innovation Center of Biomedical Functional Materials, Nanjing 210046, China

ARTICLE INFO

Article history:
Received 1 August 2014
Received in revised form
11 September 2014
Accepted 16 September 2014
Available online 20 September 2014

Keywords:
Polypyrrole
Graphene quantum dots
Dopamine
Fluorescent sensor

ABSTRACT

A facilely prepared fluorescent sensor was developed for dopamine (DA) detection with high sensitivity and selectivity based on polypyrrole/graphene quantum dots (PPy/GQDs) core/shell hybrids. The composites exhibit strong fluorescence emission, which is dramatically enhanced as high as three times than pristine GQDs. The prepared sensor allows a highly sensitive determination of DA by fluorescent intensity decreasing with the addition of DA and presents a good linearity in range of 5–8000 nM with the detection limit of 10 pM ($S/N=3$). Furthermore, the application of the proposed approach have been demonstrated in real samples and showed promise in diagnostic purposes.

1. Introduction

Dopamine (DA), a kind of neurotransmitter and hormone of the phenethylamine and catecholamine families, plays a critical role in the human body and brain (Qu et al., 2013). The dysfunctions of dopamine systems may lead to several nervous system diseases such as Parkinson's disease and schizophrenia (Wu et al., 2012). Thus, a sensitive and precise detection of DA is of great importance in the clinical diagnosis of neurological diseases. Substantial efforts have been taken to quantify the DA, including enzymatic methods (Fritzen-Garcia et al., 2013), electrochemistry (Yu et al., 2012; Biji and Patnaik, 2012; Qian et al., 2014), capillary electrophoresis (Bouri et al., 2012), high performance liquid chromatography (Syslova et al., 2011) and ultraviolet–visible spectrophotometry (J.J. Feng et al., 2013; X.M. Feng et al., 2013; Xu and Yoon, 2011). However, most of these techniques do not meet the increasing requirements for developing simpler, more reliable and more cost-efficient DA sensors (Yang and Li, 2014; Yildirim and Bayindir, 2014). Therefore, further development of high sensitivity and selectivity sensors for DA is desired. Compared with the described approaches, fluorescence spectroscopy for DA analysis, as a simple, efficient and sensitive method, is attracting great interest.

During the past decades, the semiconductor quantum dots (SQDs), a type of photoluminescent nanomaterials, have drawn extensive attention due to their good performance in cell imaging and sensing (Bruchez et al., 1998). However, the SQDs have suffered from intrinsic limitations such as heavy metals potential toxicity and environmental hazards (Valizadeh et al., 2012; Cao et al., 2007). Therefore, looking for eco-friendly alternatives has been becoming highly desirable and urgent. Recently, graphene quantum dots (GQDs), as a new-style quantum dot system, offer strong potential for promising candidates to replace traditional SQDs. GQDs are consisted of a single layer or few-layer of carbon atoms in a closely packed honeycomb structure (Jiang et al., 2013). Because of the quantum confinement and edge effects, they possess some distinct properties, such as high biocompatibility, chemical inertness, good water-solubility, stable photoluminescence and high electrical conductivity (Zhou et al., 2014; Dong et al., 2013), which suggest great potential as a new platform in photovoltaic devices and imaging fields (Li et al., 2013; Ran et al., 2013). However, the GQDs prepared for chemical sensing are few reported, probably due to the difficulty in seeking GQDs that can both selectively identify a target and give sensitive signal response (Dong et al., 2012b).

Nowadays, polypyrrole (PPy) is a booming and increscent investigated class of conjugated materials because of its excellent electronic, optical and thermal properties (Jeon et al., 2011). Also this material has been found promising application in many different fields including supercapacitors, functional electrodes and sensors (Yang et al., 2012; Chen et al., 2013; Qian et al.,

* Corresponding author. Fax: +86 83316661.
** Corresponding author at: School of Chemistry and Chemical Engineering, Nanjing University, Nanjing 210093, China. Fax: +86 83316661.
E-mail addresses: shishanwu@nju.edu.cn (S. Wu), shenj57@nju.edu.cn (J. Shen).

http://dx.doi.org/10.1016/j.bios.2014.09.038
0956-5663/

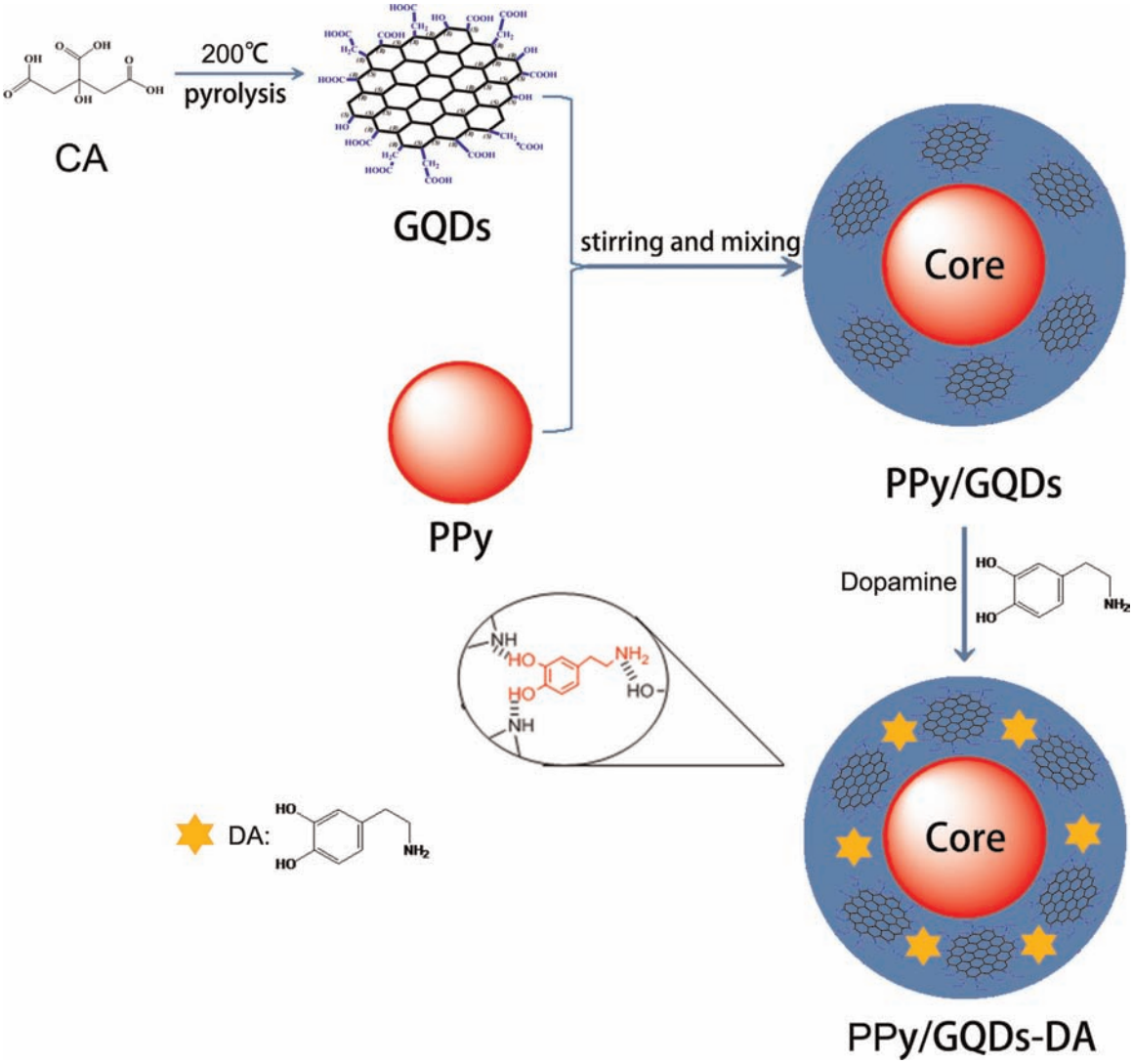

Fig. 1. Illustration of the preparation of PPy/GQDs.

2013b, 2013a; Chatterjee et al., 2013). In this study, we report a facile fabrication of PPy/GQDs core/shell composites by synthesizing GQDs in the presence of PPy microspheres (Fig. 1). The existence of amine groups on the PPy backbone may lead to enhancement of fluorescence intensity of GQDs by surface passivation (Dong et al., 2012a; Shen et al., 2012). Moreover, abundant oxygen-containing groups at the surface of PPy microspheres enable to adsorb the DA molecules effectively onto the surface of composites by interaction with amine and hydroxyl functional groups in DA through hydrogen bonds (Qian et al., 2014), thus multiply recognizing DA with high sensitivity and specificity.

2. Materials and methods

2.1. Reagents and materials

Hydrogen peroxide (H_2O_2, 30% AR) and pyrrole (AR) were purchased from Sinopharm Chemical Reagent Co. (China). NaOH (AR) and $FeCl_2$ (AR) were obtained from Shanghai Chemical Reagent Co. (China). Citric acid (AR) was purchased from Nanjing Chemical Reagent Co. Ltd. (China). Deionized water was applied for all polymerization and reaction processes. Ascorbic acid (AA), DA, uric acid (UA), norepinephrine (NE) and 3,4-dihydroxyphenylacetic acid (DOPAC) were purchased from Aladdin Chemical Reagent Co. (China). 5-Hydroxyindole acetic acid (5-HIAA) was obtained from Sigma-Aldrich Co. Human serum and urine were provided by the local hospital and stored at 4 °C.

2.2. Instruments and measurements

Fluorescence measurements were carried out on an LS SS Perkin Elmer spectrometer. UV–vis spectra were measured on a Lambda 35 Perkin Elmer spectrometer. Transmission electron microscopy (TEM) images were obtained by a JEM 2100 high-resolution TEM. Zeta potential was recorded on a Malvern Nano-Z Instrument. X-ray photoelectron spectroscopy (XPS) measurements were performed on a PHI 5000 VersaProbe. All Fourier transform infrared (FTIR) spectroscopic measurements were performed on a Nicolet NEXUS870 spectrometer.

2.3. Synthesis of the PPy microspheres

In a typical preparation procedure, PPy was initiated with the addition of 5 mL H_2O_2 to the pyrrole/$FeCl_2$/H_2O (1 mL/0.1 g/94 mL) mixture and lasted for 6 h. After that, centrifugation was used for concentrating the products, which had been washed with water several times to remove reaction byproducts and unused

reactants, the prepared PPy microspheres were dispersed in water at a concentration of 0.09 g PPy/40.00 g H_2O.

2.4. Synthesis of the PPy/GQDs core/shell composites and GQDs

PPy/GQDs were prepared by one step hydrothermal treatment citric acid (CA) to PPy/NaOH system. 2 g CA monohydrate was heated to 200 °C in a 5 mL beaker by a heating mantle, until the CA changed to a pale yellow liquid. Then, the liquid was dissolved into 100 mL of 10 mg mL^{-1} NaOH solution in the presence of 200 μL of PPy dispersion, with vigorous stirring for 3 h. The obtained solution was further neutralized with NaOH solution. Preparation processes of GQDs were as same as the approach mentioned above but without the addition of PPy dispersion. The obtained GQDs solution was further dialyzed in a dialysis bag (retained molecular weight: 3500 Da) for 48 h to obtain pristine GQDs.

2.5. Fluorescence measurements

In a typical test, PPy/GQDs solution (200 μL, pH 7.0), 0.1 mol/L PBS buffer (pH 7.0, 1 mL), and different amounts of DA or other analytes (AA, UA, NE, DOPAC, and 5-HIAA) were added into a 5 mL cuvette. Then the solution was diluted to the mark with deionized water followed by being incubated at room temperature for 30 min. Fluorescence spectra were recorded under excitation at 365 nm. The fluorescence spectra were recorded from 370 nm to 700 nm, and the slit widths of excitation and emission were both 4 nm.

2.6. Detection of real samples

Human serum and urine samples were collected from healthy laboratory volunteers at the local hospital. A quantity of the DA was added to a 100-fold diluted serum and urine samples before fluorescent analysis and no other pretreatments were necessary. The content of the DA was determined by the standard addition method.

3. Results and discussion

3.1. Characterization of composites

As a class of organic conductive materials, PPy could combine with nanomaterials such as GQDs, and apply in the construction of optical, electrical and biomedical device. The combination of these two interesting materials may bring many advantages such as good fluorescence intensity and nice sensitivity. In this work, a core/shell hybrid based on PPy and GQDs was developed. The optical properties of composites were characterized by the fluorescence and UV–vis absorption spectroscopy, shown in Fig. 2A. The fluorescence intensity of PPy/GQDs is three times higher than the free GQDs, which probably owing to the surface passivation of GQDs through an acid–base type interaction between the carboxylic groups of GQDs and the nitrogen atom of PPy (Routh et al., 2013; Dong et al., 2012a). Additionally, the PPy microspheres are probably beneficial for accumulating the incompletely carbonized citric acid at the periphery of composites through π–π interaction, which could surface passivate GQDs (Dong et al., 2012a, 2012b).

The PPy/GQDs present a fluorescence emission peak at 465 nm and an excitation peak at 365 nm. Furthermore, FTIR spectral analysis was used to characterize the construction of composites. In Fig. 3A, both GQDs and PPy/GQDs exhibit one characteristic peak at about 3416 cm^{-1}, which is ascribed to the hydroxyl groups linked to the composites. PPy/GQDs have the characteristic peaks at 1560 and 2922 cm^{-1} due to the –COOH and $-CH_2$ bonding vibration. PPy has a characteristic peak at about 1400 cm^{-1} for the C–N bonding vibration, but in the PPy/GQDs composites, this peak shifts from 1400 to 1394 cm^{-1} because of protonation from the carboxylic acid group of GQDs (Routh et al., 2013; Dong et al., 2012b). At the same time, compared with the spectra of PPy/GQDs, there is no new peak appeared in the spectra of the PPy/GQDs–DA complex. However, stretching vibration peak of O–H broaden, which could be attributed to the hydrogen bond interaction of DA with PPy/GQDs. Moreover, the morphology of composites were presented by TEM (Fig. 3B–D), which display a microsphere structure of PPy with typically smooth surface and the monodispersed nanoparticles of GQDs distributed in the range of 3–7 nm, respectively. A representative high-resolution TEM (HRTEM) image of an individual GQDs presents more details in the inset of Fig. 3C. TEM micrographs of PPy/GQDs samples are presented in Fig. 3D, which shows that GQDs are present at the periphery of PPy microspheres and displays an interesting feature of distinct core/shell morphology. This may be attributed to the π–π interaction between the PPy and the sp^2 π clouds of GQDs (Routh et al., 2013; Li et al., 2013). Moreover, the diameters of the PPy/GQDs are mainly distributed in the range of 950–1775 nm with an average diameter of 1.43 ± 0.21 μm (the inset of Fig. 3D).

3.2. The interactions between DA and PPy/GQDs

Fig. 2B shows the typical excitation (curve a) and emission (curve b) spectra of PPy/GQDs. Upon adding DA to the PPy/GQDs, the fluorescence of PPy/GQDs is quenched greatly (Fig. 2B, curves c

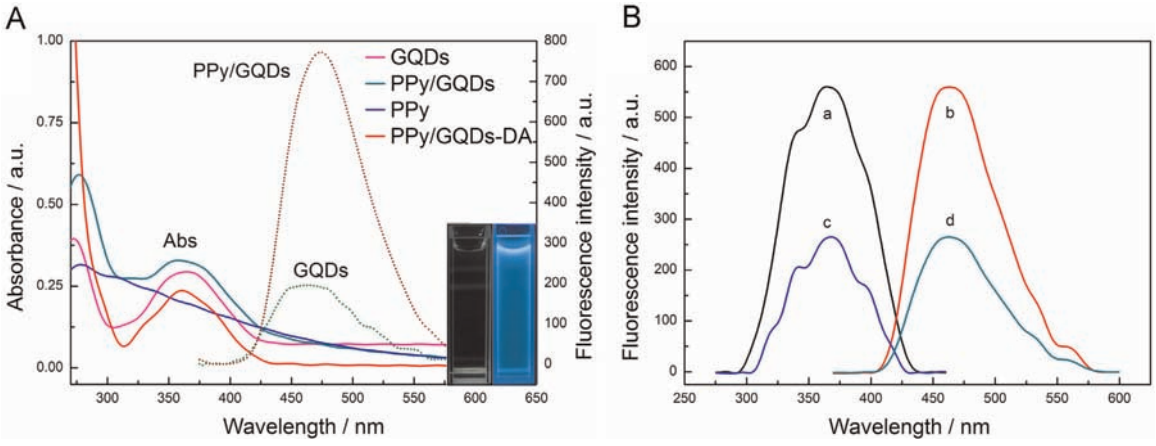

Fig. 2. (A) UV–vis absorption spectra of PPy, GQDs and PPy/GQDs. Fluorescence emission spectra of GQDs and PPy/GQDs (inset: the fluorescent image of PPy/GQDs hybrids). (B) The excitation (a, c) and emission (b, d) fluorescence spectra of the PPy/GQDs in the absence (a, b) and presence (c, d) of 10 μM DA.

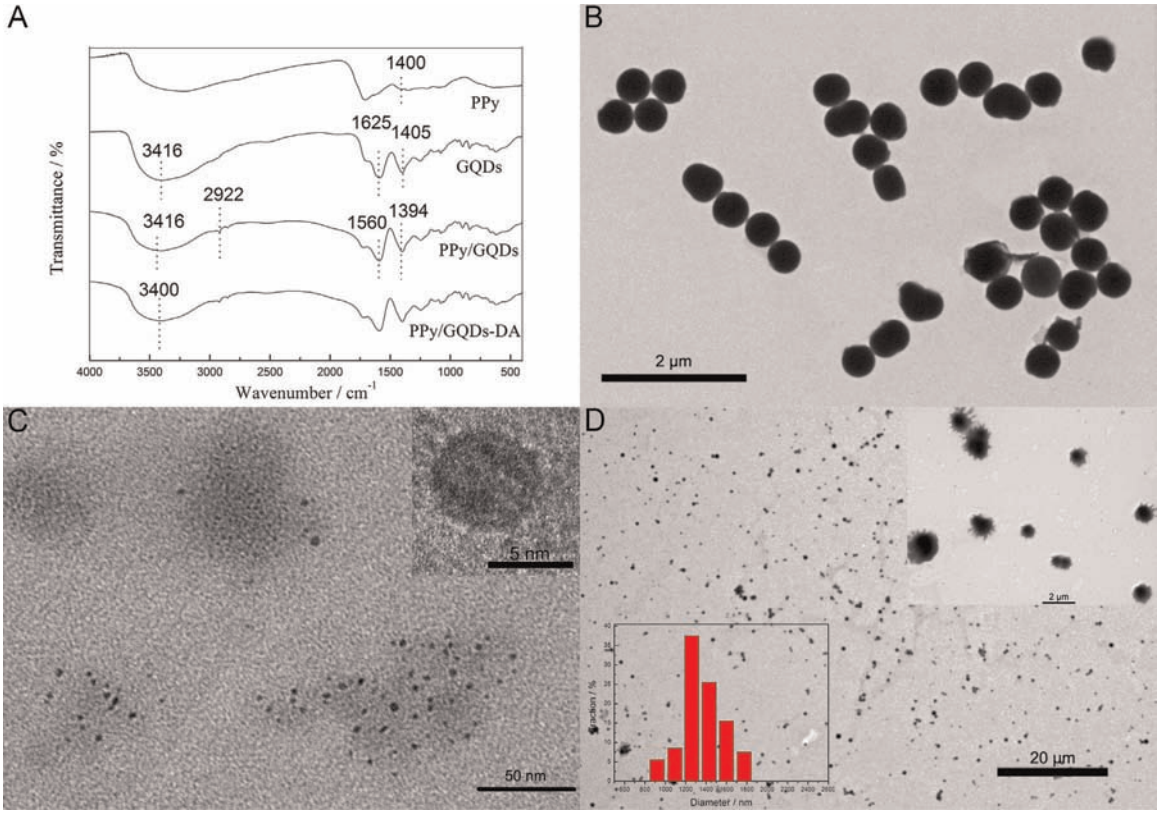

Fig. 3. The FTIR spectra (A) of the PPy, GQDs, PPy/GQDs and PPy/GQDs–DA. The TEM images of (B) PPy, (C) GQDs (inset: HRTEM image of GQDs) and (D) PPy/GQDs (upper right inset: enlarged TEM image of the core/shell structure of PPy/GQDs, bottom left inset: the corresponding size distribution of PPy/GQDs).

and d), indicating that the PPy/GQDs could employ as a highly efficient fluorescent sensor for DA analysis.

We studied the influence of pH value, which is of great importance to the fluorescence intensity of fluorescence sensors. On one hand, the pH value may affect the fluorescence response of PPy/GQDs. As shown in Fig. 4A (blue columns), fluorescence intensity of PPy/GQDs is obviously pH dependent and relatively low in acidic solutions, which is unfavorable for developing a stable and sensitive sensing strategy. In contrast, the fluorescence intensity of PPy/GQDs reaches a maximum and keeps stable in neutral and alkaline conditions. On the other hand, pH value may affect the form of DA in water. It has been reported that in a weak alkaline solutions, dopamine will undergo self-polymerization to produce an adherent polydopamine (PDA), with the accompanied oxidation of catechol groups to the quinone form, which is a disadvantage in accurate detection of DA (Lee et al., 2008). As shown in Fig. 4B, an increase of the pH value from 7.0 to 8.0 leads to a decreased of the F_0/F value. That is to say, the fluorescence intensity of PPy/GQDs is relatively insensitive to the change of concentration of DA in alkaline solutions, which confirms the effect in detection of DA caused by self-polymerization of DA. Therefore, neutral conditions (pH 7.0) are suitable for this sensing system.

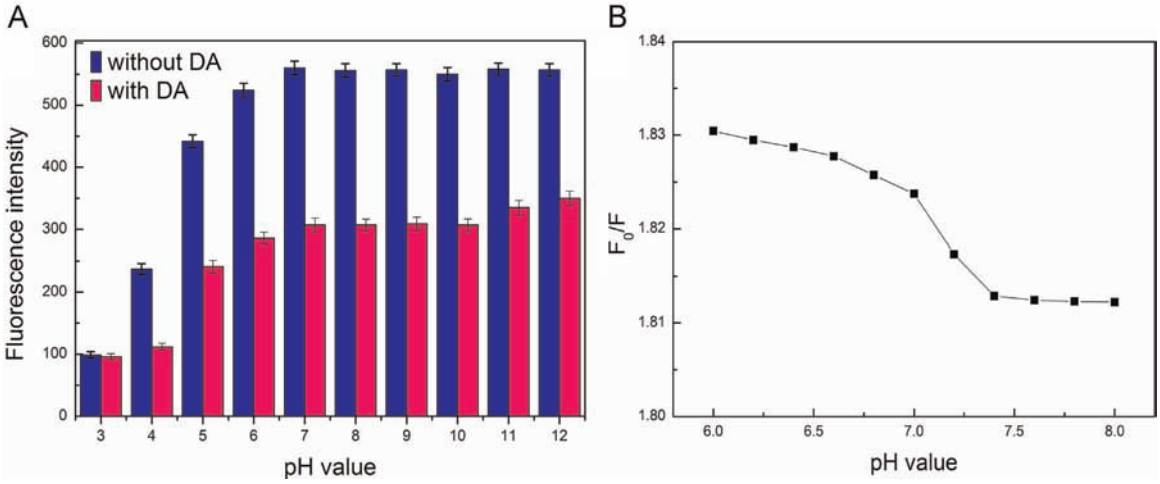

Fig. 4. Fluorescence responses of the PPy/GQDs in the absence and presence of 10 μM DA at different pH values (A: histogram, B: linear graph). F_0 and F are the fluorescence intensity of PPy/GQDs in the absence and presence of DA, respectively. (For interpretation of the references to color in this figure legend, the reader is referred to the web version of this article.)

3.3. Mechanism of DA induced fluorescence quenching of PPy/GQDs

Recently, substantial efforts have been made on the applications of GQDs for the development of sensing systems based on the changes of fluorescence intensity because of the photo-induced electron transfer (PET) (Qu et al., 2013), fluorescence resonance energy transfer (FRET) (Zhou et al., 2014), or other interactions occurring at the GQDs surface (Lu et al., 2013). There is no overlap between the absorption spectrum of DA and the emission spectrum of PPy/GQDs, which weakens the FRET as a possible mechanism for PPy/GQDs fluorescence quenching. Additionally, from the UV spectra and FTIR spectra, the possibility of surface reaction could be ruled out for the formation of PPy/GQDs–DA via noncovalent interactions. Moreover, we measured the zeta potential of PPy/GQDs before and after addition of DA. A significant reduction of the zeta potential from −21.9 mV of free PPy/GQDs to −13.5 mV of PPy/GQDs in the presence of 10 μM DA at pH 7.0 shows the strong electrostatic interaction between PPy/GQDs and DA. Meanwhile, the pH dependent quenching efficiency of DA also confirms the charges screening effect of the PPy/GQDs (Fig. 4). Thus, the quenching effect presumably results from the photo-induced electron transfer. When the amine and hydroxyl functional groups of DA interacts with the oxygen-containing groups in PPy/GQDs, the lone pair of electrons in the oxygen-containing groups is available for intramolecular charge transfer or photo-induced electron transfer, leading to a decrease of the emission (Bouri et al., 2012; Song et al., 2011).

3.4. Fluorescent properties of composites

The further research about the fluorescence quenching effect of DA on fluorescence intensity of PPy/GQDs is revealed in Fig. 5, which shows the relationship between DA concentration and the fluorescence intensity of PPy/GQDs. As reported in the previous literatures (Liu et al., 2013), the fluorescence quenching of QDs towards DA can be described by a Stern–Volmer type equation:

$$F_0/F = 1 + K_{sv}C_{DA}$$

where F_0 and F are the fluorescence intensities in the absence and presence of a quencher (DA is the quencher in this study), respectively, K_{sv} is the quenching constant of the quencher, and C_{DA} is the concentration of DA.

Fig. 5B displays a good linear correlation between F_0/F and the concentration of DA in the range of 5–8000 nM with a correlation coefficient of $R^2=0.9992$. The limit of detection (LOD) for DA is as low as 10 pM based on the signal corresponding to three times the noise of the response. The slope of the calibration plot of proposed sensor for DA is 0.083, which is much higher compared to that obtained by GQDs (slope: 0.007, in Fig. 5B). As shown in Table 1, the results of PPy/GQDs sensor for detecting DA are compared with that of other published quantum dots-based sensors, which demonstrated high sensitivity and low detection limit of the prepared PPy/GQDs sensor, indicating the superiority of such composites.

Table 1
The comparison of different quantum dots-based fluorometric sensors for DA determination.

Materials	Detection limit (nM)	Linear range (μM)	Reference
Au@CDs-CS[a]	1	0.1–100	Huang et al. (2013)
APTES-capped ZnO QDs [b]	12	0.05–10	Zhao et al. (2013)
CDs-CS[c]	11.2	0.1–30	Huang et al. (2013)
F-CuInS$_2$ QDs[d]	200	0.5–40	Liu et al. (2013)
CNPs/Fe^{3+}[e]	68	0.1–10	Qu et al. (2013)
PPy/GQDs	0.01	0.005–8	This work

[a] Composite of Au modified carbon quantum dots–chitosan.
[b] ZnO quantum dots capped by (3-aminopropyl) triethoxysilane.
[c] Carbon quantum dots and chitosan composite sensor.
[d] CuInS$_2$ ternary quantum dots capped by mercaptopropionic acid sensor.
[e] Carbon nanoparticles and Fe^{3+} hybrid sensor.

3.5. Detection of DA in real samples

To investigate the applicability and reliability of the proposed biosensor, the standard addition method was used to test DA in human serum and urine samples. The results are shown in Table 2. The recoveries of DA were found to be in the range of 97.65–103.28%, and the relative standard deviation (RSD) was lower than 2.27%. The above results are probably due to strong electrostatic interaction between the electronegative parts of PPy/GQDs and the electropositive parts of DA. Additionally, hydrogen bonds interaction between the amine groups or the phenolic hydroxyl groups in DA and the nitrogen heteroatoms in PPy/GQDs is another force for selectively attracting DA onto the surface of composites (J.J. Feng et al., 2013; X.M. Feng et al., 2013; Qian et al., 2014; Tsai et al., 2012). It demonstrates that the proposed aptasensor is appropriate for the practical application in clinical determination of DA.

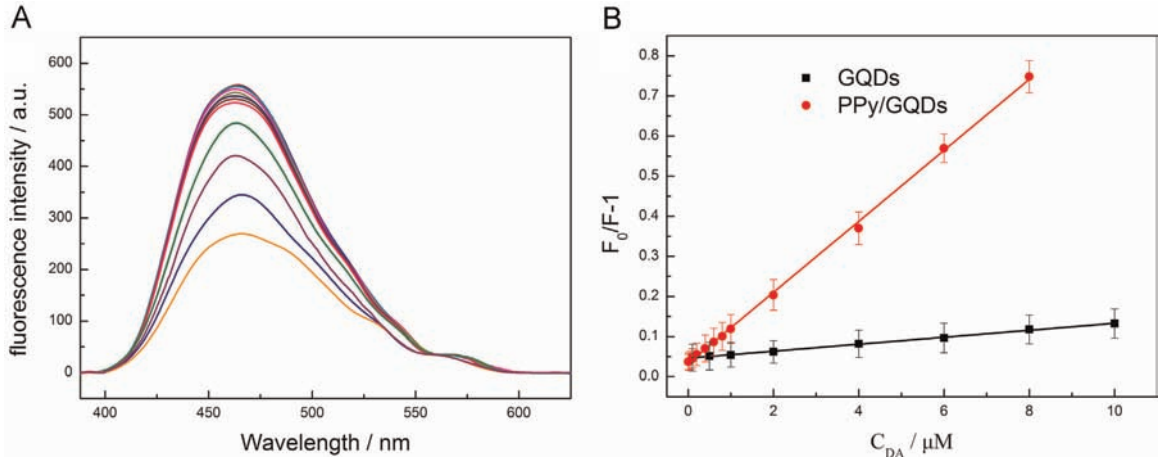

Fig. 5. (A) The fluorescence emission spectra of increasing DA concentration, DA concentration was 0.005, 0.01, 0.05, 0.1, 0.2, 0.4, 0.6, 0.8, 1, 2, 4, 6 and 8 μM (from top to bottom), respectively (B) The calibration curve of DA obtained with PPy/GQDs and GQDs.

Table 2
Determinations of DA in human serum and urine samples.

Sample	Spike (nM)	Found (nM)	Recovery (%)	RSD ($n=3$, %)
Serum	50.00	51.05	102.10	1.75
	100.00	101.35	101.35	0.86
	500.00	492.65	98.53	1.52
	1000.00	978.80	97.88	1.47
	2000.00	2024.80	101.24	2.13
Urine	50.00	49.20	98.40	0.89
	100.00	97.65	97.65	2.27
	500.00	505.45	101.09	1.69
	1000.00	990.50	99.05	0.98
	2000.00	2065.6	103.28	1.73

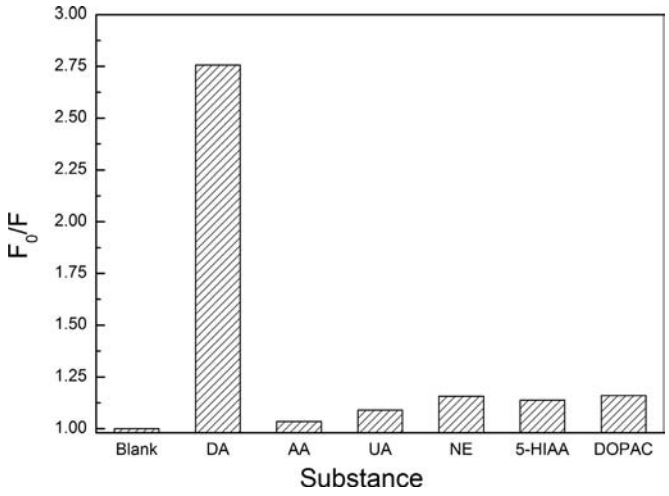

Fig. 6. Effect of a series of 10 μM physiological molecules (DA, AA, UA, NE, 5-HIAA, DOPAC) on the fluorescence intensity of PPy/GQDs. F_0 and F are the fluorescence intensity of PPy/GQDs in the absence and presence of physiological molecules, respectively.

3.6. *Effect of other biomolecules*

Along with the sensitivity requirement, high specificity is a matter of necessity especially in real sample detection. To verify whether the proposed sensor is specific for detection DA, the fluorescent signals from common molecules including AA, UA, DOPAC, NE and 5-HIAA were investigated and compared with that of DA at the same concentration. From Fig. 6, it was found that a selective quenching effect by DA over other species in the present assay. Therefore, the developed novel sensor offers high selectivity for DA because of the strong noncovalent interactions between DA and PPy/GQDs, of which the electronegative parts could reject these anions such as UA ($pK_a=5.75$) and 5-HIAA ($pK_a=4.7$) (Tsai et al., 2012).

4. Conclusion

In summary, we report a core/shell hybrid of GQDs by using citric acid and PPy. More importantly, we have demonstrated a new type of sensor based on PPy/GQDs for detection of DA with high selectivity and sensitivity. This assay has several significant features. Firstly, the method relies on the fluorescence quenching through a photo-induced electron transfer (PET) process. It is simple in design and economic in operation, which eliminates the demand for sophisticated equipments and experimental techniques. Secondly, the assay provides a convenient "mix-and-detect" protocol for homogeneous and rapid determination of DA. Furthermore, the proposed strategy is successfully applied to the detection of DA in real samples. And the new approach eliminates the need to use organic dyes, SQDs, which are much more eco-friendly. Therefore, we expect that this approach may offer a new strategy for developing simple, low cost and sensitive sensors for detecting of DA, and will be beneficial for biological and environmental applications.

Acknowledgments

This work was supported by the National Natural Science Foundation of China (Nos. 51272100 and 51273073) and the Foundation of Jiangsu Collaborative Innovation Center of Biomedical Functional Materials.

Appendix A. Supplementary information

Supplementary data associated with this article can be found in the online version at http://dx.doi.org/10.1016/j.bios.2014.09.038.

References

Biji, P., Patnaik, A., 2012. Analyst 137, 4795–4801.
Bouri, M., Lerma-Garcia, M.J., Salghi, R., Zougagh, M., Rios, A., 2012. Talanta 99, 897–903.
Bruchez, M., Moronne, M., Gin, P., Weiss, S., Alivisatos, A.P., 1998. Science 281, 2013–2016.
Cao, L., Wang, X., Meziani, M.J., Lu, F., Lin, Y., Harruff, B.A., Veca, L.M., Murray, D., Xie, S.Y., Sun, P., 2007. J. Am. Chem. Soc. 129, 1318–1319.
Chatterjee, S., Shit, A., Nandi, A.K., 2013. J. Mater. Chem. A 1, 12302–12309.
Chen, H., Shao, L., Li, Q., Wang, J.F., 2013. Chem. Soc. Rev. 42, 2679–2724.
Dong, Y.Q., Li, G.L., Zhou, N.N., Wang, R.X., Chi, Y.W., Chen, G.N., 2012a. Anal. Chem. 84, 8378–8382.
Dong, Y.Q., Wang, R.X., Li, H., Shao, J.W., Chi, Y.W., Lin, X.M., Chen, G.N., 2012b. Carbon 50, 2810–2815.
Dong, Y.Q., Pang, H.C., Yang, H.B., Guo, C.X., Shao, J.W., Chi, Y.W., Li, C.M., Yu, T., 2013. Angew. Chem. Int. Ed. 52, 7800–7804.
Feng, J.J., Guo, H., Li, Y.F., Wang, Y.H., Chen, W.Y., Wang, A.J., 2013a. ACS Appl. Mater. Interfaces 5, 1226–1231.
Feng, X.M., Zhang, Y., Yan, Z.Z., Chen, N.N., Ma, Y.W., Liu, X.F., Yang, X.Y., Hou, W.H., 2013b. J. Mater. Chem. A 1, 9775–9780.
Fritzen-Garcia, M.B., Monteiroa, F.F., Cristofolini, T., Zanetti-Ramos, B.G., Soldi, V., Pasa, A.A., Creczynski-Pasa, T.B., 2013. Sens. Actuat. B Chem. 182, 264–272.
Jeon, S.S., Kim, C., Ko, J., Im, S.S., 2011. J. Mater. Chem. 21, 8146–8151.
Jiang, F., Chen, D., Li, R., Wang, Y., Zhang, G., Li, S., Zheng, J., Huang, N., Gu, Y., Wang, C., Shu, C., 2013. Nanoscale 5, 1137–1142.
Lee, H.S., Lee, Y.H., Statz, A.R., Rho, J.S., Park, T.G., Messersmith, P.B., 2008. Adv. Mater. 20, 1619–1623.
Li, L.L., Wu, G., Yang, G., Peng, J., Zhao, J., Zhu, J.J., 2013. Nanoscale 5, 4015–4039.
Liu, S.Y., Shi, F.P., Zhao, X.J., Chen, L., Su, X.G., 2013. Biosens. Bioelectron. 47, 379–384.
Lu, J.J., Yan, M., Ge, L., Ge, S.G., Wang, S.W., Yan, J.X., Yu, J.H., 2013. Biosens. Bioelectron. 47, 271–277.
Qian, T., Yu, C.F., Wu, S.S., Shen, J., 2013a. Biosens. Bioelectron. 50, 157–160.
Qian, T., Zhou, X., Yu, C.F., Wu, S.S., Shen, J., 2013b. J. Mater. Chem. A1, 15230–15234.
Qian, T., Yu, C.F., Zhou, X., Ma, P.P., Wu, S.S., Xu, L.N., Shen, J., 2014. Biosens. Bioelectron. 58, 237–241.
Qu, K.G., Wang, J.S., Ren, J.S., Qu, X.G., 2013. Chem.—A Eur. J. 19, 7243–7249.
Ran, X., Sun, H., Pu, F., Ren, J., Qu, X., 2013. Chem. Commun. 49, 1079–1081.
Routh, P., Das, S., Shit, A., Bairi, P., Das, P., Nandi, A.K., 2013. ACS Appl. Mater. Interfaces 5, 12672–12680.
Shen, J.H., Zhu, Y., Yang, X., Li, C., 2012. Chem. Commun. 48, 3686–3699.
Song, F.Y., Ma, X., Hou, J.L., Huang, X.B., Cheng, Y.X., Zhu, C.J., 2011. Polymer 52, 6029–6036.
Syslova, K., Rambousek, L., Kuzma, M., Najmanova, V., Valesova, V.B., Slamberova, R., Kacer, P., 2011. J. Chromatogr. A 1218, 3382–3391.
Tsai, T.C., Han, H.Z., Cheng, C.C., Chen, L.C., Chang, H.C., Chen, J.J., 2012. Sens. Actuat. B Chem. 171-172, 93–101.
Valizadeh, A., Mikaeili, H., Samiei, M., Farkhani, S.M., Zarghami, N., Kouhi, M., Akbarzadeh, M., Davaran, S., 2012. Nanoscale Res. Lett. 7, 1–14.

Wu, L., Feng, L.Y., Ren, J.S., Qu, X.G., 2012. Biosens. Bioelectron. 34, 57–62.
Xu, Q.L., Yoon, J.Y., 2011. Chem. Commun. 47, 12497–12499.
Yang, C., Xu, C., Wang, X., 2012. Langmuir 28, 4580–4585.
Yang, Y.J., Li, W.K., 2014. Biosens. Bioelectron. 56, 300–306.
Yildirim, A., Bayindir, M., 2014. Anal. Chem. 86, 5508–5512.
Yu, D.J., Zeng, Y.B., Qi, Y.X., Zhou, T.S., Shi, G.Y., 2012. Biosens. Bioelectron. 38, 270–277.
Zhou, Y., Qu, Z.B., Zeng, Y.B., Zhou, T.S., Shi, G.Y., 2014. Biosens. Bioelectron. 52, 317–323.